Int. J. Heat Mass Transfer. Vol. 9, pp. 17–34. Pergamon Press 1966. Printed in Great Britain

NON-EQUILIBRIUM TRANSPORT PHENOMENA OF PARTIALLY IONIZED ARGON

M. N. BAHADORI† and S. L. SOO‡
Department of Mechanical Engineering, University of Illinois, Urbana, Illinois

(*Received* 20 *January* 1965 *and in revised form* 15 *June* 1965)

Abstract—Non-equilibrium transport properties of partially ionized argon and the nature of relaxation of electrons at a cooled surface were studied with measurements made on a steady flow two-dimensional arc-heated channel. Study consists of extension of boundary-layer theory to the case of flow of an ionized gas over a cooled wall, and evaluation of transport properties by an iterative solution of equations of momentum integral method. Results show that although the atom and ion temperatures decrease significantly toward the cooled wall, the electron temperature, concentration, and the thermal and electrical conductivities stay at much higher values than those based on equilibrium electron concentration.

NOMENCLATURE

- a, passage height;
- a_j, coefficient of series expansion of equation (21);
- b, half-passage width;
- b_j, coefficient of series expansion of equation (20);
- c_j, coefficient of series expansion of equation (19);
- c_p, specific heat at constant pressure;
- D_e, diffusion coefficient of electrons;
- D_e^T, thermal diffusion coefficient of electrons;
- E, electric field;
- E_r, energy of radiation per unit volume per unit time;
- f, $= m_e/m_a$;
- $f(\eta^*)$, function defined by equation (19);
- $g(\eta)$, function defined by equation (20);
- $g_e(\eta_e)$, function defined by equation (21);
- H_e, enthalpy of electrons, given by $h_e + V_i$;
- h, enthalpy; heat-transfer coefficients;
- I, current;
- J, current density;
- k_e, rate constant for electron production;
- k_e^*, rate thickness;
- k_r, recombination rate;
- $\dot{m}$, flow rate;
- m_e, mass of electrons ;
- m_a, mass of ions;
- Nu_b, Nusselt number;
- n_e, concentration of electrons;
- n_i, concentration of ions;
- P, pressure;
- Pr, Prandtl number of the fluid;
- Q_x, energy crossing a section;
- Q_y, energy crossing the wall at a section;
- Re_b, Reynolds number;
- T, temperature;
- T_e, electron temperature;
- t, time;
- u, x-component of velocity;
- V_{ey}, electron drift velocity;
- V_i, ionization potential;
- v_e, electron thermal velocity;
- x, axis of direction of flow;
- y, axis normal to x and measured from the wall.

Greek symbols

- α, extent of ionization;
- δ, boundary-layer thickness, velocity;
- δ_u, velocity thickness;
- δ^*, displacement thickness;
- δ_1, defined by equation (14);
- Δ, boundary-layer thickness, temperature;

† Present address: Assistant Professor of Mechanical Engineering, Department of Mechanical Engineering, University of Missouri, Rolla, Missouri.

‡ Professor of Mechanical Engineering.

Δ_e, boundary-layer thickness, concentration;
Δ_1, defined by equation (16);
Δ_{e1}, defined by equation (18);
η, defined by equation (15);
η^*, defined by equation (13);
η_e, defined by equation (17);
η_p, ratio of T_e/T;
θ, momentum thickness;
θ_e, concentration thickness;
θ_H, enthalpy thickness;
λ, thermal conductivity;
μ, viscosity;
ρ, density of gas;
σ, electrical conductivity;
σ_{ea}, collision cross-section of electrons with atoms;
σ^*, electric conductivity thickness.

Subscripts
1, core outside the boundary layer;
w, wall.

Superscript
$'$, quantity based on equilibrium composition.

INTRODUCTION

NON-EQUILIBRIUM transport properties, especially thermal and electrical conductivities, are significant in the est mation of the requirements and effects of cooling (by ablation or convection) during spacecraft re-entry and in magnetohydrodynamic generators and accelerators. The present study treats the simple model of partially ionized argon with determination of its non-equilibrium transport properties with measurements made on a laminar two-dimensional flow system [1–3]. Results also demonstrate feasibility of applying the present method to other gases and those with more complex molecules.

Boundary-layer motion of a dissociated or ionized gas has been studied by numerous investigators: Fay [8] considered the mechanism of heat transfer and determined a similarity variable for the stagnation point boundary layer; Lees [4], Kemp, Rose and Detra [5], dealt with the problems of heat transfer to highly cooled walls; the case of ionized gas has been considered by Rossow [6], Shohet *et al.* [7], Fay [8], Meksyn [9], Tani [10], Hains and Yoler [11], and Moffat [12] in their treatments of flow of conducting fluid, neglecting temperature gradient; Cann [13] made measurements of heat transfer from an ionized gas to a cylinder; the case of heat transfer to a cooled wall was studied by Novack and Brogan [14]. In all cases, local thermal and electrical conductivities of the gas were either not measured [13, 14] or assumed constant [6], or assumed to follow equilibrium ionization which can be approximated by a stepwise change [2]. The possibility of taking the difference between electron temperature and ion temperature into account was suggested by Lam [15].

Emmons and Land [2] first suggested that simultaneous flow of a gas and electric current through a tube (Poiseuille motion) provides an experimental arrangement for the study of the properties of an ionized gas. Their experiment gave mean (discontinuous) plasma properties. The present study, with a rectangular-duct model, permits measurements of local temperature (optical method) and ion concentration (spectroscopic method).

When a partially ionized gas is not at thermal equilibrium condition, due to finite recombination rate [16], the electron concentration will remain above that at thermal equilibrium at the cooled wall. Further, the electron temperature will not follow the atom and ion temperatures in their decrease toward the wall temperature, but will remain at a higher value due to the ineffectivness of energy exchange by collision of electrons and other particles. Thus, even if the free stream is at near equilibrium, the above relaxation of electron states should be accounted for in estimating heat transfer from an ionized gas to a cooled surface. All these aspects are shown below.

Our experimental study was made with the choice of low velocity steady flow of an ionized gas so that substantial effect of boundary-layer thickness is felt while the effect of aerodynamic heating is negligible; and the choice of high enough pressure such that continuum flow is maintained but with the arc maintained at relatively low temperature below 10^4°K by a known electric field for sustained experimental runs. This combination assures that the relaxation of the electron state will be felt in the measurements.

EXPERIMENTAL SYSTEM

The "two-dimensional" arc heated channel with 4·75 mm × 34 mm passage consists of sections of water-cooled copper plates separated from each other by transite and bakelite sheets as shown in Fig. 1. The operating pressures

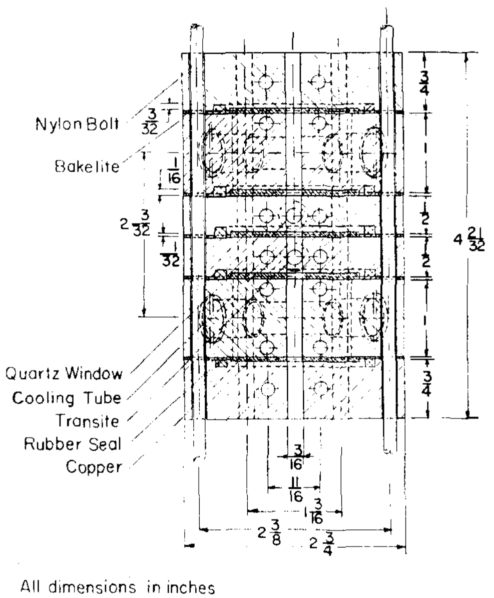

FIG. 1(a). Test section.

range from 250 mm Hg to 750 mm Hg. Four pairs of electrodes are each powered individually by two 200 V, 15 amp, current controlled power supplies (Spectrometer Industries). The discharge is longitudinal in the direction of flow. Such an arrangement assures uniform electric field (E) across the channel at the section where measurements were made. A typical voltage distribution is shown in Fig. 2. The ion concentration and gas radiation were monitored by an 82-00 Ebert grating type monochromator (Jarrel Ash). The details [23] are abstracted in Appendix A. Evaporation of wall materials was checked constantly among spectral lines during test runs; none were found in the operating range. Density gradients in the gas were measured with a mercury light source of an a.c. wave pattern produced by a light chopper of 600 c/s; the optical system is shown in Fig. 3. A typical measurement of light beam deflection is shown

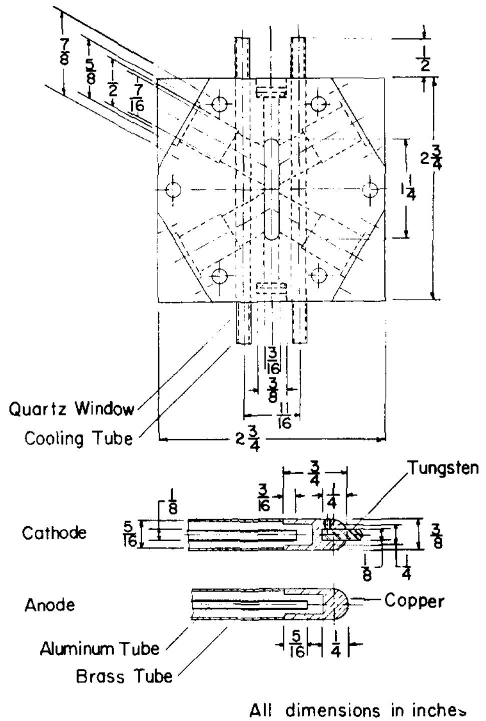

FIG. 1(b). Test section, top view and detail of electrodes.

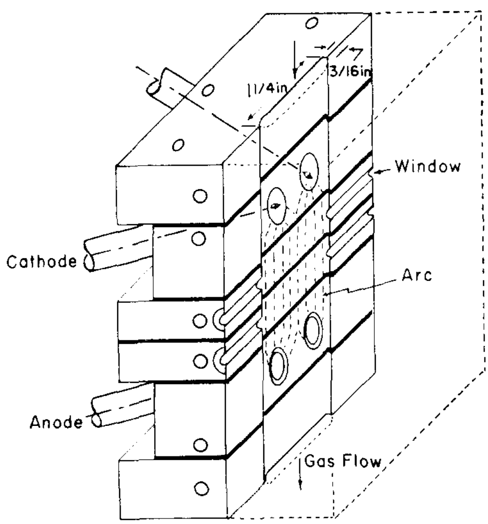

FIG. 1(c). Cutaway view of test section with electrodes in position.

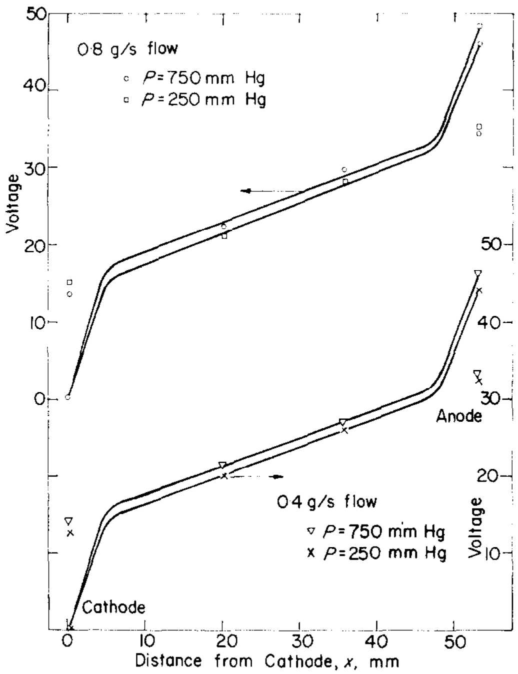

FIG. 2. Voltage drop across the discharge gap.

in Fig. 4. Other measurements are wall temperatures (chromel–alumel thermocouples), potential, and overall gas flow, water flow, their temperatures, as well as the overall current and voltage. Argon gas was used in all the experiments. Low flow velocities (10–60 m/s) were used to maintain substantial boundary layer thickness (about 1 to 3 mm) for convenience of measurement. The maximum gas temperature reached was 7750°K at 0·4 g/s and 60 m/s. The effect of natural convection was shown to be negligible [17].

BASIC RELATIONS

The above experimental system (Fig. 1) is capable of rigorous formulation because:

(*a*) the velocity distribution and boundary-layer thickness in the region ahead of the cathode can be computed based on potential motion [19] and momentum integral method [17];

(*b*) between the electrodes and away from the region in the vicinity of the electrodes, the electric field is uniform and accurately measured (Fig. 2). The temperature of the ionized gas in the core (away from the boundary layer) is nearly constant. The small passage width ($2b = 4{\cdot}75$ mm) limits radiation to the case of a thin emitter (at a spectrograph temperature of, say, 5000°K, the range of wave length is 3000 Å–8000 Å), and the heat loss due to radiation can be calculated from numerical integration of measured spectra [18]. The magnitude of heat transfer by radiation in the present system is below 10^3 W/m^3 at 6000°K;

(*c*) Owing to the small extent of ionization ($\alpha < 10^{-3}$), the momentum and sensible energy of the fluid and its viscosity is unaffected by electronic states, although the electrical and thermal conductivities are strongly influenced by the electronic states.

After some derivations from the basic differential equations of continuity, momentum, energy and extent of ionization of the present reactive system as outlined by Hirschfelder, Curtis and Bird [20], followed by momentum

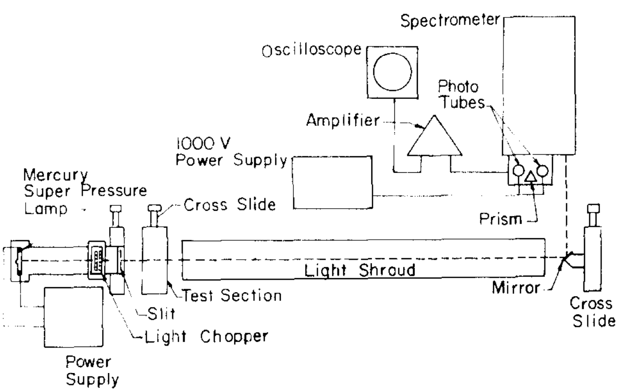

FIG. 3. Schematic diagram of the optical system.

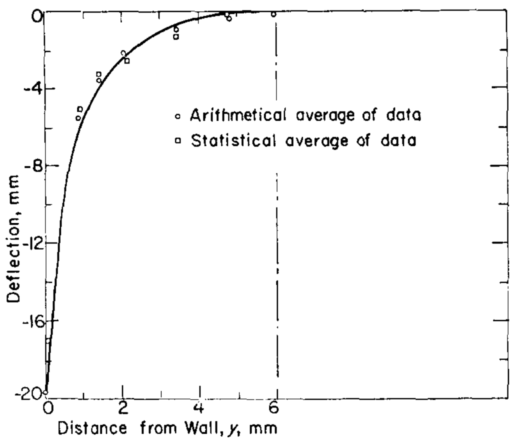

FIG. 4. Light beam deflection due to gas temperature gradient [1].

integral method [17], the above considerations give:

$$\frac{d\theta}{dx} + \frac{\theta}{u_1}\frac{du_1}{dx}\left(2 + \frac{\delta^*}{\theta}\right) + \frac{\theta}{\rho_1}\frac{d\rho_1}{dx} = \frac{\mu_w}{\rho_1 u_1^2}\frac{\partial u}{dy}\bigg|_w \tag{1}$$

$$\frac{d}{dx}(\rho_1 u_1 h_1 \theta_H) - \rho_1 u_1 \theta_H \frac{dh_1}{dx} = \int_0^b \left[\mu\left(\frac{\partial u}{\partial y}\right)^2 + (EJ - E_r) - \frac{u}{u_1}(EJ_1 - E_{r1})\, dy - \frac{\mu_w}{Pr_w}\frac{\partial h}{\partial y}\right]_w + [H_e n_e V_{ey}]_w \tag{2}$$

and

$$\frac{d}{dx}(\rho_1 u_1 \alpha_1 \theta_e) - \rho_1 u_1 (\delta^* - k_e^*) = \left[\rho D_e \frac{\partial \alpha}{\partial y} - \frac{\rho}{m_e}\frac{D_e^T}{nT}\frac{\partial T}{\partial y}\right]_w \tag{3}$$

where x is in the direction of flow, y is normal to x and measured from the wall; ρ, u, h, α are density, x-component of velocity, enthalpy, and extent of ionization of the gas; and subscript 1 is for the free stream (core); E is the electric field, J is the current density, E_r is the energy of radiation per unit volume per unit time, μ_w and Pr_w are the viscosity and the Prandtl number of the fluid at the wall (subscript 2); H_e is the enthalpy of the electrons given by $h_e + eV_i$, V_i being the ionization potential; n_e is the electron concentration, V_{ey} is the electron drift velocity; D_e is the diffusion coefficient of electrons and D_e^T is the thermal diffusion coefficient of electrons. For half-passage width b, the boundary-layer integrals are:

the momentum thickness:

$$\theta = \int_0^b \frac{\rho u}{\rho_1 u_1}\left(1 - \frac{u}{u_1}\right) dy \tag{4}$$

the displacement thickness:

$$\delta^* = \int_0^b \left(1 - \frac{\rho u}{\rho_1 u_1}\right) dy \tag{5}$$

the enthalpy thickness:

$$\theta_H = \int_0^b \frac{\rho u}{\rho_1 u_1}\left(\frac{T}{T_1} - 1\right) dy \tag{6}$$

the concentration thickness:

$$\theta_e = \int_0^b \frac{\rho u}{\rho_1 u_1}\left(\frac{\alpha}{\alpha_1} - 1\right) dy \tag{7}$$

and the rate thickness:

$$k_e^* = \int_0^b \left(1 - \frac{k_e}{k_{e1}}\right) dy \tag{8}$$

where k_e is the rate constant for electron production [13]. Further, the condition in the core is given by:

$$\frac{dP}{dx} = -\rho_1 u_1 \frac{du_1}{dx} \tag{9}$$

where P is the pressure, and

$$\rho_1 u_1 c_p \frac{dT_1}{dx} - \rho_1 u_1 \frac{du_1}{dx} = E^2\sigma_1 - E_{r1} \tag{10}$$

where c_p is the specific heat at constant pressure, and σ is the electrical conductivity. The overall dissipation in the passage is given by:

$$IE = 2aE^2 \int_0^b \sigma\, dy \tag{11}$$

where I is the current and a is the passage height.

Simultaneous solution of equations (1), (2) and (3) can be carried out by introducing the velocity thickness

$$\delta_u = \delta^* - \theta_H = \int_0^b \left(1 - \frac{\rho u h}{\rho_1 u_1 h_1}\right) \mathrm{d}y = \int_0^b \left(1 - \frac{u}{u_1}\right) \mathrm{d}y \quad (12)$$

which is also a modified enthalpy thickness; and transforming the coordinate y to

$$\eta^* = \frac{1}{\delta_1} \int_0^y \frac{\rho}{\rho_1} \mathrm{d}y \quad (13)$$

$$\delta_1 = \int_0^\delta \frac{\rho_1}{\rho} \mathrm{d}y \quad (14)$$

$$\eta = \frac{1}{\Delta_1} \int_0^y \frac{\rho}{\rho_1} \mathrm{d}y \quad (15)$$

$$\Delta_1 = \int_0^\Delta \frac{\rho_1}{\rho} \mathrm{d}y \quad (16)$$

$$\eta_e = \frac{1}{\Delta_{e1}} \int_0^y \frac{\rho}{\rho_1} \mathrm{d}y \quad (17)$$

$$\Delta_{e1} = \int_0^{\Delta_e} \frac{\rho_1}{\rho} \mathrm{d}y \quad (18)$$

(where δ, Δ, Δ_e are thicknesses of the velocity, temperature and concentration profiles measured from the wall to the edge of the core (Figs. 9 and 10) by polynomials with undetermined coefficients and

$$\frac{u}{u_1} = f(\eta^*) = \sum c_j \eta^{*j} \quad (19)$$

$$\frac{T}{T_1} = g(\eta) = \sum b_j \eta^j \quad (20)$$

$$\frac{\alpha}{\alpha_1} = g_e(\eta_e) = \sum a_j \eta_e{}^j \quad (21)$$

For our experimental range ($T_1 \sim 5000°$K, $T_w \sim 1000°$K), the term $[H_e n_e V_{ey}]_w$ in equation (2) is of order 10^{-2} while $(\mu_w/Pr_w)(\partial h/\partial y)_w$ is of order 10^2 at $T \sim 5000°$K; thus the term $[H_e n_e V_{ey}]_w$ can be neglected. Low velocities in our experiments permit dropping the dissipation term $\mu_w(\partial u/\partial y)^2$ from equation (2). With these simplifications, equations (1) and (2) are now independent of equation (3). Equations (1) and (2) are solved simultaneously by an iterative procedure.

We further introduce an electric conductivity thickness,

$$\sigma^* = \int_0^b \left(1 - \frac{\sigma}{\sigma_1}\right) \mathrm{d}y \quad (22)$$

which gives

$$IE = 2aE^2\sigma_1 \int_0^b \frac{\sigma}{\sigma_1} \mathrm{d}y = 2aE^2\sigma_1(b - \sigma^*) \quad (23)$$

or

$$\int_0^b \left(EJ - EJ_1 \frac{u}{u_1}\right) \mathrm{d}y = E^2\sigma_1 \int_0^b \left(1 - \frac{u\sigma}{u_1\sigma_1}\right) \mathrm{d}y = E^2\sigma_1(\delta_u - \sigma^*) \quad (24)$$

The total flow rate is given by:

$$\dot{m} = 2a \int_0^b \rho u \, \mathrm{d}y = 2a\rho_1 u_1(b - \delta^*) \quad (25)$$

For given E, I, T_w, P, flow rate $\dot{m}$ and cooling losses, iterative solution (starting with $\sigma(T)$ for equilibrium thermal ionization [21]) of equations (1) and (2) takes the steps as given in the Appendix, taking $j = 0, 1$ in equations (19) and (20).

For the experimental data given in Table 1, $\delta(x)$ is given in Fig. 5, $\Delta(x)$ in Fig. 6, $T_1(x)$ in Fig. 7, $u_1(x)$ in Fig. 8, $u(x, y)$ in Fig. 9, and $T(x, y)$ in Fig. 10; $\sigma(T, T_e)$ in Fig. 11, $\lambda(T, T_e)$ in Fig. 12; $\mu(T)$ in Fig. 13 (showing the general degree of consistency with available data of Amdur and Mason [22]), $\alpha(T, T_e)$ in Fig. 14; $n_e(T)$, $\alpha(x, y)$, $n_e(x, y)$ in Figs. 15 and 16. Figures 11, 12, and 14 give the corresponding σ,

Table 1. Experimental data

Flow rate, $\dot{m}$ (g/s)	0·8			0·4			0·84 (Ref. 1)
Pressure, p (mm Hg)	750	500	250	750	500	250	750
Density. ρ, at 300°K (Kg/m³)	1·67	1·11	0·55	1·67	1·11	0·55	1·67
Overall voltage drop, V_t	46	50·8	48·5	44	48·5	46·5	57
Cathode voltage drop, V_c	15·7	16·5	17·3	14·6	15·3	16·0	20·0
Positive column voltage drop, V_p	17·0	16·6	16·2	16·2	15·8	15·45	14·4
Electric field at cathode, E_c (V/cm)	3·14	33·0	34·6	29·2	30·6	32·0	40
Electric field at positive column, E_p (V/cm)	3·96	3·86	3·77	3·77	3·68	3·59	2·62
Current carried by gas, I	58·5	65	68·5	66	70	73	80
Heat loss to cathodes, Q_c (W)	350	400	500	400	450	500	400
Heat loss to anodes, Q_A (W)	700	750	850	750	800	900	800
Heat loss to walls, Q_w (W)	900	1320	1500	1250	1360	1540	1700
Wall temperature, T_w	660	600	560	710	650	610	500 1000

λ, and α in this experimental case with comparison to other experimental data. In these figures, η_p is the ratio T_e/T, T_e being the electron temperature, and point to point correspondence was maintained. The derivation leading to the curves parametric with η_p was reported in the thesis by Tan [23], based on the method of Chen, Leiby and Goldstein [24], and of Berger, Bernstein, Frieman and Kulsrud [25]. $\eta_p = 1$ gives α', λ', σ' at equilibrium states of the partially ionized gas.

RELAXATION OF ELECTRON TEMPERATURE

From the data obtained for the electrical and thermal conductivities and the extent of ionization (Figs. 11–16), it is seen that, due to

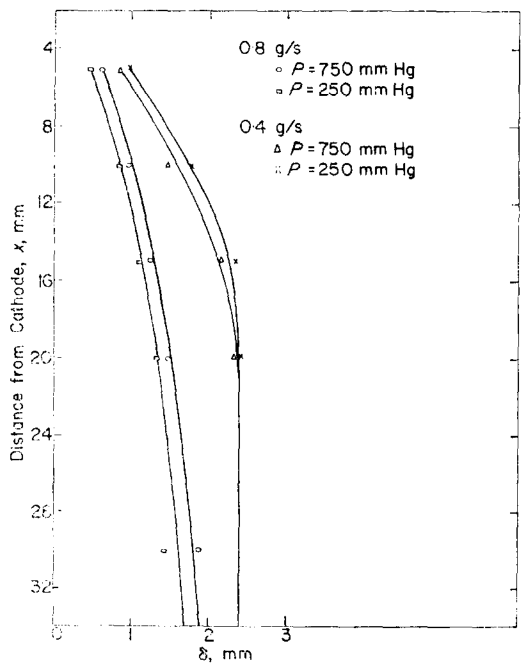

FIG. 5. Velocity boundary-layer thickness, δ.

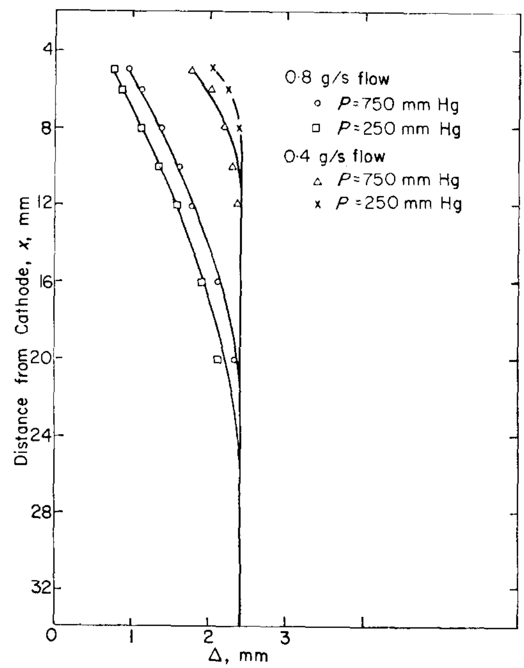

FIG. 6. Temperature boundary-layer thickness, Δ.

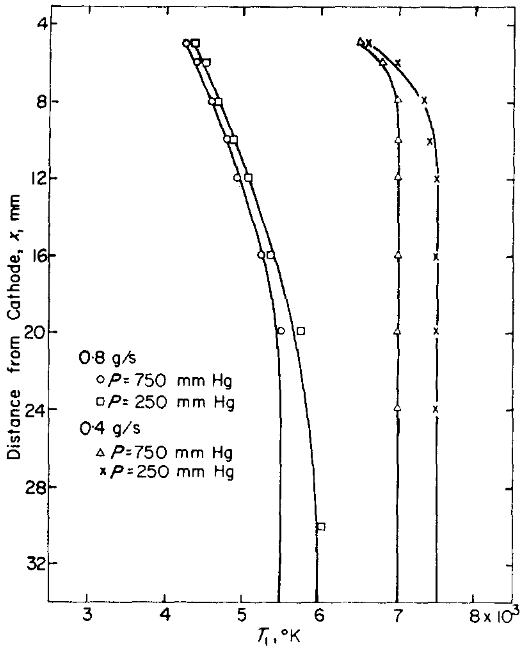

FIG. 7. Free stream gas temperature, T_1.

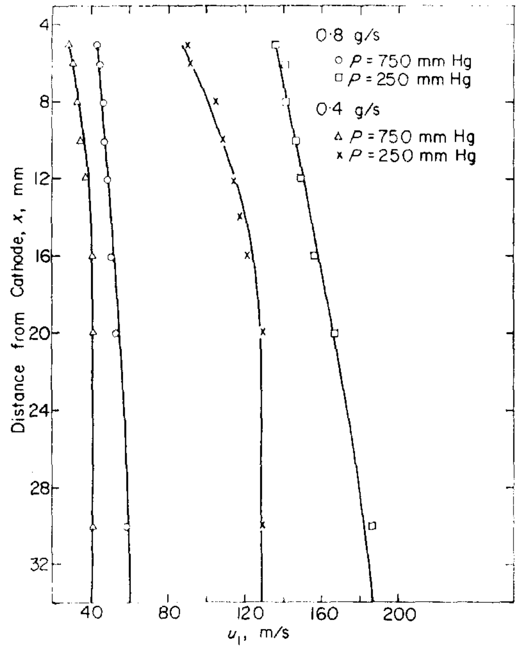

FIG. 8. Free stream velocity, u_1.

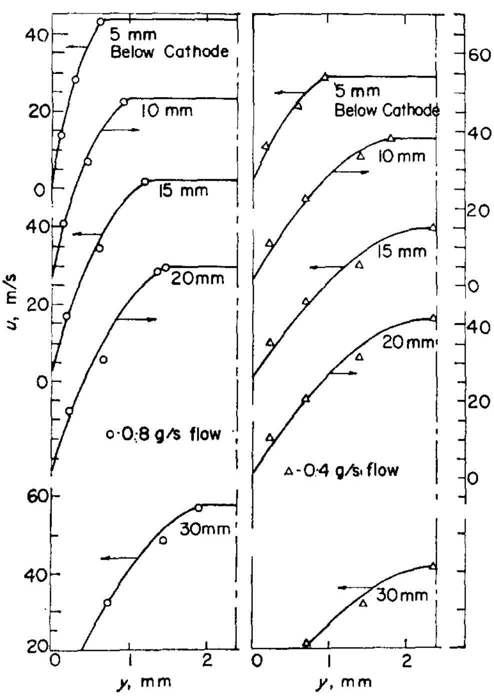

FIG. 9. Velocity profiles at $P = 750$ mm Hg.

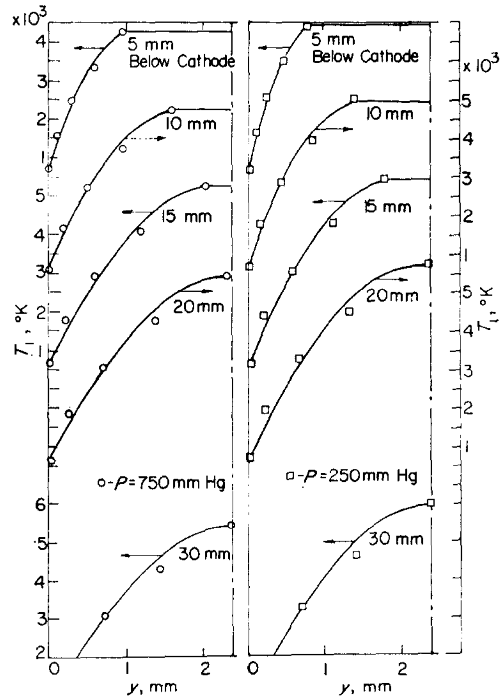

FIG. 10. Temperature profiles for 0·8 g/s flow.

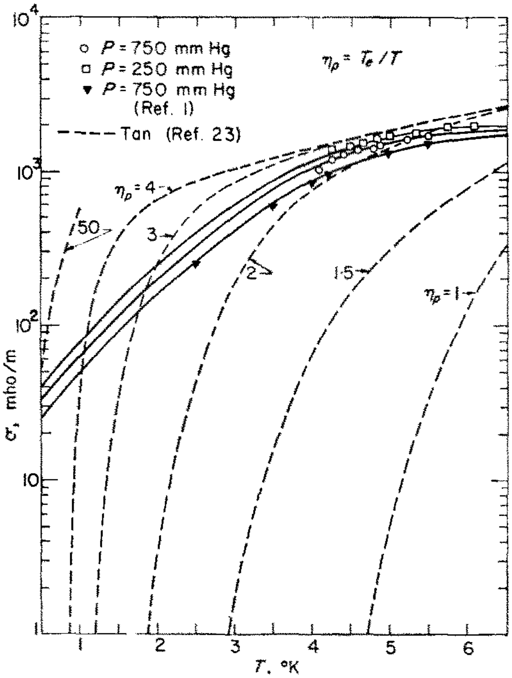

FIG. 11. Electrical conductivity, σ, for 0·8 g/s flow rate.

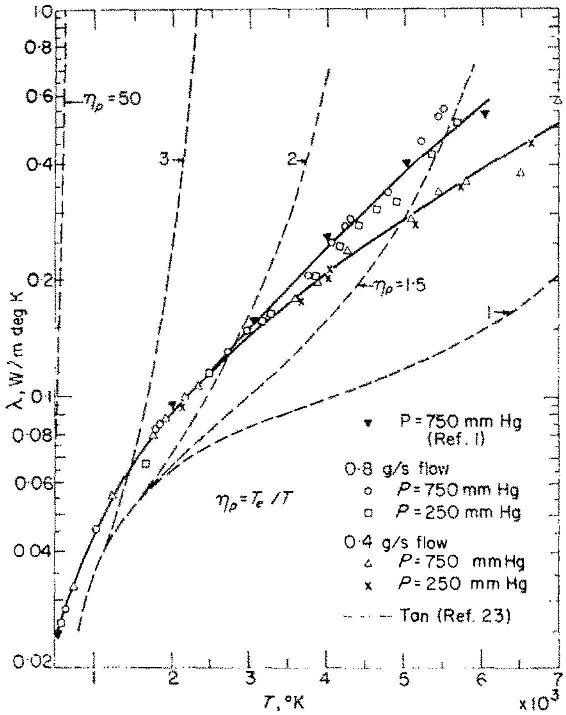

FIG. 12. Thermal conductivity, λ.

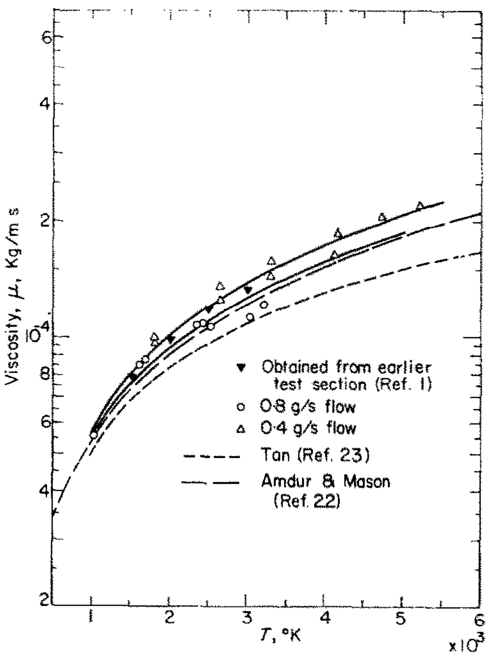

FIG. 13. Viscosity, μ, at 750 mm Hg pressure.

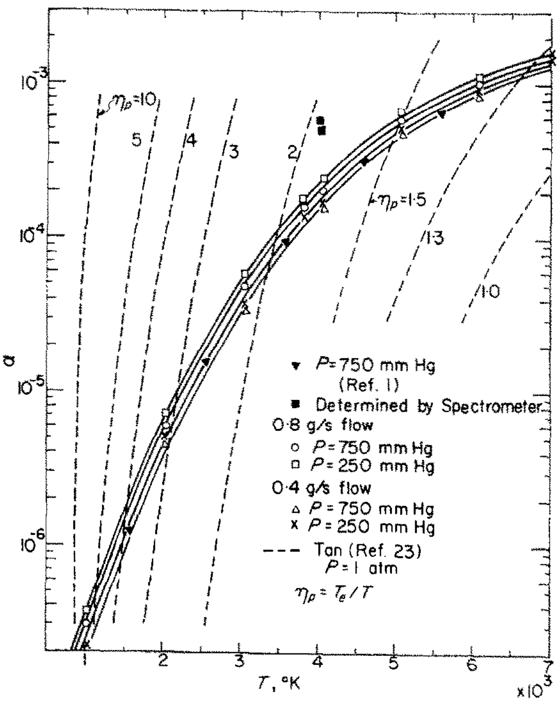

FIG. 14. Extent of ionization, α.

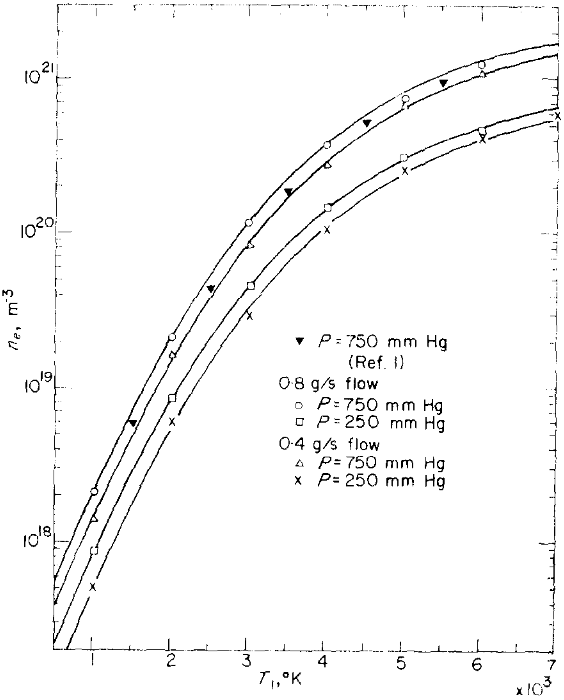

FIG. 15. Electron concentration, n_e.

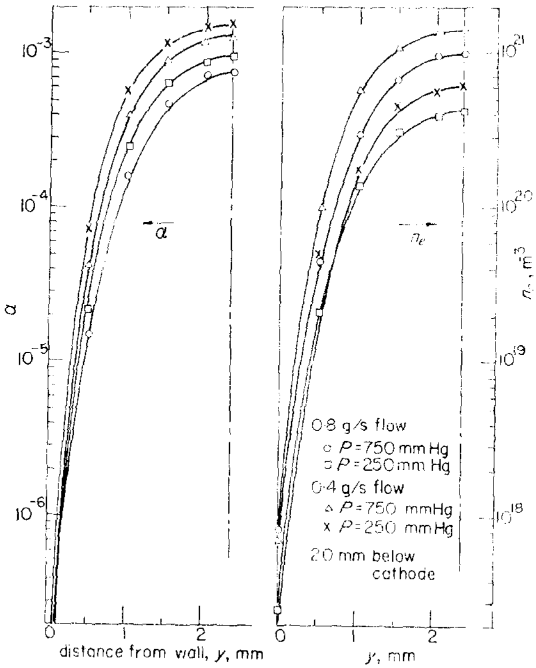

FIG. 16. Electron density and extent of ionization profiles.

deviation from equilibrium states in the rate processes, the value of $\eta_p = T_e/T$ increases toward the cooled walls, while both electron and gas temperatures decrease. Since the heat removed by cooling (mainly from translational energy of atoms and ions) is far greater than the heat released by recombination, the decrease in electron temperature may be attributed to elastic collisions of electrons only. Based on formulation by Compton and Langmuir [26], we can determine the electron temperature drop toward the wall from

$$\frac{\mathrm{d}T_e}{T_e} = -\frac{1}{4} f Z \frac{\mathrm{d}y}{V_{ey}} \tag{26}$$

where f is the fraction of energy lost by electrons at each collision, Z the collision frequency, V_{ey} the diffusion velocity of electrons toward the wall, which may be written as

$$V_{ey} = -D \frac{1}{n_e} \frac{\partial n_e}{\partial y} \tag{27}$$

where D is the electron diffusion coefficient. By substituting for D in terms of electron mobility K_e [26, 27],

$$D = \frac{K_e}{e} k T_e = 0{\cdot}85 \sqrt{2} \frac{1}{\pi r^2 n} \frac{kT_e}{m_e \bar{v}_e} \tag{28}$$

where r is the atomic radius ($1{\cdot}82 \times 10^{-10}$ m) and, for Z,

$$Z = \bar{v}_e \pi r^2 n = \sqrt{\left(\frac{8}{\pi} k \frac{T_e}{m_e}\right)} \pi r^2 n \tag{29}$$

and for f,

$$f = 2{\cdot}66 \frac{m_e}{m_a} \left(1 - \frac{T}{T_e}\right) \tag{30}$$

into equation (26), we obtain:

$$\frac{T_{ew}}{T_{e1}} = \exp\left[-1{\cdot}10 \times 10^{13} P^2 \times \int_0^{\Delta} \left(1 - \frac{T}{T_e}\right) \frac{n_e}{T^2} \frac{\mathrm{d}y}{(\partial n_e/\partial y)}\right] \tag{31}$$

where P is in atmospheres, n_e in m^{-3}. The integrand in equation (31) is a function of y, and

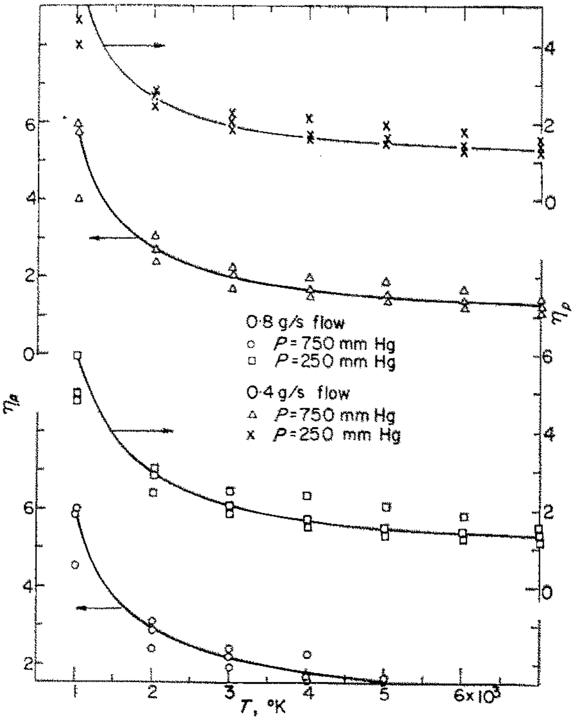

FIG. 17. Ratio of electron to gas temperature, $\eta_p = T_e/T$.

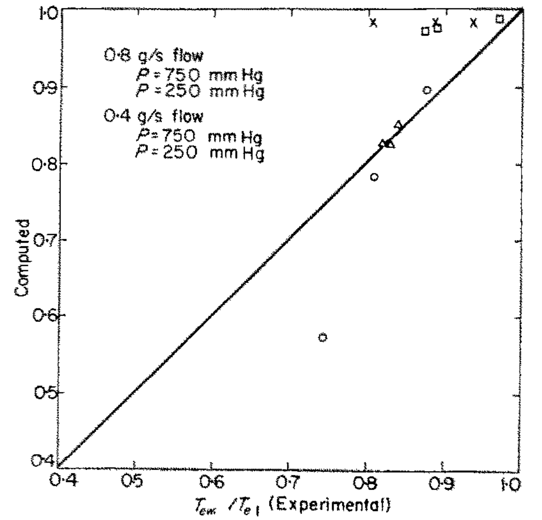

FIG. 18. Relaxation of electron temperature in the boundary layer.

thus the integration may be performed graphically. The values of T_{ew}/T_{e1} obtained from equation (31), plotted against those obtained experimentally (Fig. 17), are shown in Fig. 18.

DETERMINATION OF RECOMBINATION COEFFICIENT

Recombination of electron and ion is determined from

$$\frac{dn_e}{dt} = -k_r n_e^2 \tag{32}$$

where k_r is the recombination coefficient. Equation (32) may be integrated over the temperature boundary layer thickness, Δ, to give

$$\frac{1}{n_{ew}} - \frac{1}{n_{e1}} = -\int_0^{\Delta} k_r \frac{dy}{V_{ey}} \tag{33}$$

Substituting equations (27) and (28) in equation (33) gives

$$\frac{1}{n_{ew}} - \frac{1}{n_{e1}} = 2{\cdot}56 \times 10^5 P \times \int_0^{\Delta} k_r \frac{n_e}{T\sqrt{(T_e)}} \frac{dy}{(\partial n_e/\partial y)} \tag{34}$$

where P is in atmospheres and n_e is in m^{-3}, k_r in m^{3}s^{-1}. k_r is a function of n_e, T_e and pressure. To evaluate the recombination coefficient k_r, we replace equation (34) by

$$\frac{1}{n_{e(2j)}} - \frac{1}{n_{e(2j+2)}} = 2{\cdot}56 \times 10^5 P \times \left[k_r \frac{n_e}{(\partial n_e/\partial y)} \frac{1}{T\sqrt{(T_e)}}\right]_{2j+1} \Delta y \tag{35}$$

where j is an index. By selecting a value for Δy within the boundary layer, we can evaluate

$$\frac{n_e}{T\sqrt{(T_e)}} \frac{1}{(\partial n_e/\partial y)}$$

at y_{2j+1} (see Appendix B). The left side of equation (35) is known, and thus k_r at y_{2j+1} is determined. We have selected $\Delta y = 2$ mm and obtained k_r as a function of T_e, n_e, corresponding to y_{2j+1}. Figure 19 gives k_r as a function of T_e. The values of k_r obtained by other investigators [28, 16] are also shown with n_e and P at which the data were obtained. From the data

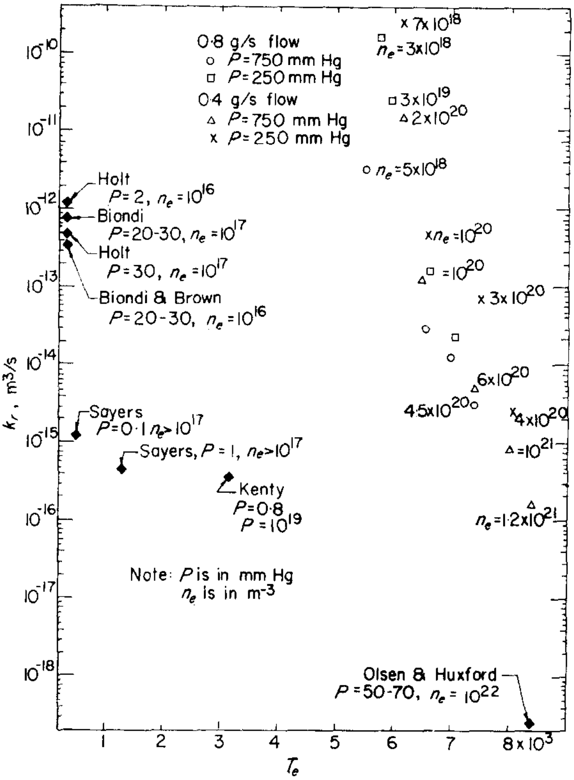

FIG. 19. Recombination coefficient, k_r, as a function of T_e.

obtained in this work (and that of the others) we note that k_r increases as T_e, P, and n_e decrease.

HEAT TRANSFER MEASUREMENTS IN THE THERMAL ENTRANCE REGION

The heat losses to the wall are determined by measuring the rate and temperature rise of the cooling water (Table 1). Figure 20 gives the average Nusselt number at the thermal entrance region. The analytical results due to Sparrow [29] and Stephan [30] which are for constant properties of gas are plotted in this figure. Figure 21 shows $Nu_b = 2b[(\partial T/\partial y)_w/(T_1 - T_w)]$ as a function of $Re_b = 2b[(\rho_1 u_1)/(\mu_1)]$, and Fig. 22 gives the variation of the Prandtl number, $Pr_1 = c_p(\mu_1/\lambda_1)$, and Nu_b as functions of distance from the cathode, x. Figure 21 also includes data obtained for the test section as reported before [1]. Values of $Nu_b = 5{\cdot}7$ and $Nu_b = 3{\cdot}8$ for the test section at fully developed flow are due to Clark and Kays [31]. High values of Nu_b at 5 and 10 mm below the cathode indicate the significance of the entrance section.

DISCUSSION

The general trend of boundary-layer motion of a partially ionized gas is shown in Fig. 23,

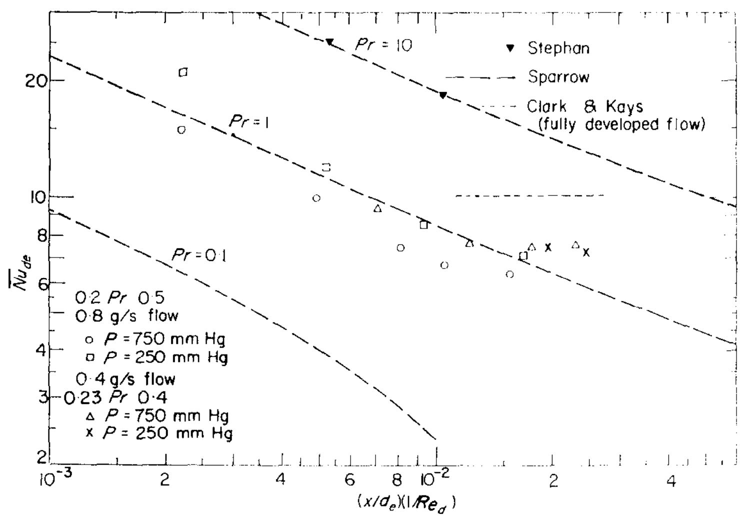

FIG. 20. Variation of average Nusselt number for the thermal entrance region.

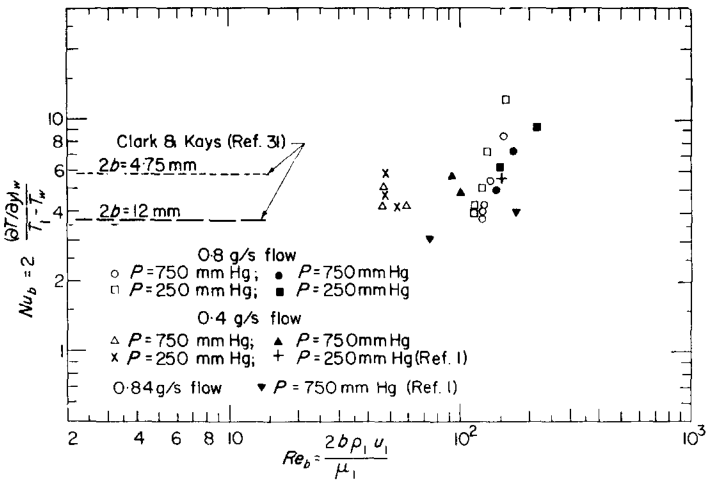

FIG. 21. Variation of Nusselt number vs. Reynolds number.

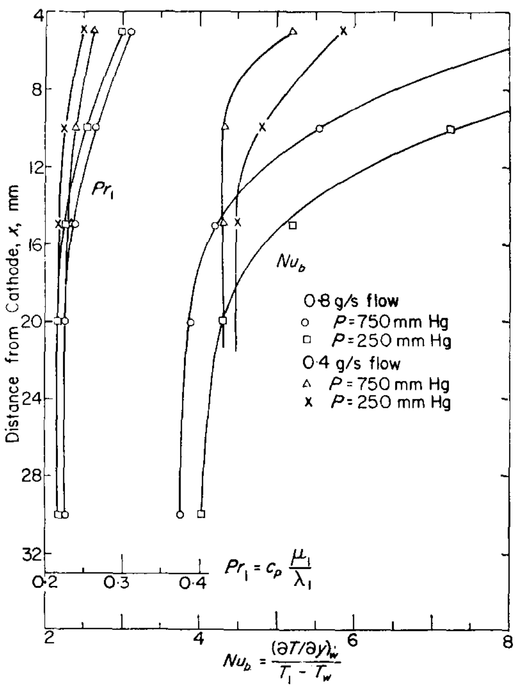

FIG. 22. Nusselt and Prandtl numbers as functions of x.

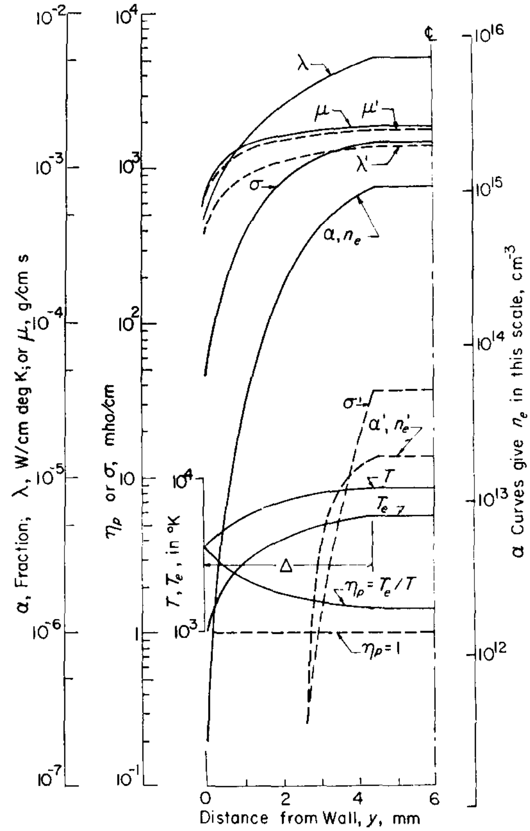

FIG. 23. T, T_e, η_p, α, λ, μ, σ, n_e, at $x = 30$ mm below cathode as compared to α', λ', σ', μ' if $T_e = T(\eta_p = 1)$ (0·8 g/s argon flow).

which gives data of T, T_e, η_p, α, n_e, σ, μ, λ, at $x = 30$ mm from the cathode in the case of our experiment. It is seen that, due to deviation from equilibrium states in the rate process, the value of $\eta_p = T_e/T$ increases toward the cooled wall, while both T and T_e decrease toward the wall. The values of η_p are consistent for all values of α, λ, and σ. Figure 17 shows the general trend of η_p vs. T for all experiments. The wide range of η_p at the wall is because of different rates of cooling near the wall. Although the atom temperature T decreases toward the wall to 1000°K, substantial values of λ and σ are maintained. For the given values T, if equilibrium states ($T = T_e$) between electrons, ions and atoms are maintained, the values of electron concentration, electrical conductivity, and thermal conductivity would be given by α' (and n_e'), σ' and λ' as shown by the dotted line in Fig. 23. (μ' and μ are not really different. Their values in Fig. 23 simply show the degree of approximation.)

From another point of view, had we assumed $T = T_e$ in computing boundary-layer flow, a much thinner thermal boundary-layer thickness and lower values of heat transfer would have been predicted, and σ' would decrease to practically zero a distance away from the cooled wall [2].

The transport properties σ and λ and the extent of ionization obtained by making use of the boundary layer developments thus found, are higher [2, 22, 32] than the values given for the case of thermally ionized gas, particularly in the boundary layer. The difference is attributed to non-equilibrium conditions in the boundary layer. That is, while both electron and gas temperature relaxation determined experimentally is compared with that obtained by considering the loss of energy of electrons due to their elastic collisions [1].

The electron–ion recombination coefficient is determined from data obtained on T, T_e, and n_e within the boundary layer. The recombination coefficient evaluated here (for the range of $5500 < T_e < 8500$°K and $10^{18} < n_e < 10^{21}\,\text{m}^{-3}$) is compared with that of others [16]. The data show that k_r increases as T_e, p and n_e decrease.

The heat transfer in the thermal entrance region of the duct was determined experimentally and compared with analytical solutions given by Stephan [30] and Sparrow [31] for the case of constant properties.

CONCLUSIONS

Study of the boundary-layer motion of a partially ionized gas is a useful means in predicting semi-experimentally the transport properties, electron temperature, and electron–ion recombination coefficient of a partially ionized gas. To solve the integral equations of motion, energy and diffusion one may utilize computers by using different profiles for temperature, velocity and concentration, and comparing the results of the transport properties and recombination coefficient for each set of profiles for their further refinements. By making use of the temperature profile, one can determine the index of refraction of the partially ionized gas by measuring the light beam deflection through the gas. The significance of thermal entrance on Nusselt number may be determined semi-experimentally based on the temperature and velocity profiles used and the heat loss measurements.

The study of the interaction of a partially ionized gas with a cooled wall shows that non-equilibrium states and properties due to electron relaxation have to be considered. When applied to the problem of re-entry, substantial electrical and thermal conductivities, not too much lower than those of the ionized gas behind the shock wave, exist at a cooled wall, although the gas temperature decreases significantly toward the wall.

ACKNOWLEDGEMENTS

The authors wish to thank Prof. H. W. Emmons for his suggestions on our experimental system in 1960, and to express their gratitude for the support of the National Science Foundation, which has made this study possible. The authors are also indebted to the Fluid Dynamics Panel, AGARD, NATO, for the opportunity to participate at the Specialist's Meeting at Rhode-Saint Genese, Sept. 21–23, 1964, which contributed to discussions.

REFERENCES

1. S. L. Soo and N. M. Bahadori, Boundary layer motion in two-dimensional arc heated channel. *AGARDograph* (NATO), **84**, 1013–1051 (1964).
2. H. W. Emmons and R. I. Land, Poiseuille plasma experiment. *Phys. Fluids* **5**, 1489–1500 (1962).

3. C. W. TAN, S. L. SOO, M. N. BAHADORI, Transport properties of non-equilibrium ionized argon gas, *Z. Angew. Math. Phys.* **16,** 255 (1965).
4. L. LEES, Laminar heat transfer near blunt-nosed bodies at hypersonic flight speeds, *Jet Propul.* **26,** 259–269 (1956).
5. N. H. H. KEMP, P. H. ROSE and R. W. DETRA, Laminar heat transfer around blunt bodies in dissociated air, *J. Aerospace Sci.* **26,** 421–430 (1956).
6. V. J. ROSSOW, On the flow of electrically conducting fluids over a flat plate in the presence of a transverse magnetic field, *NASA TR*-1358 (1958).
7. J. L. SHOHET, J. F. OSTERLE and F. J. YOUNG, Velocity and temperature profiles for a laminar magnetohydrodynamic flow in the entrance region of a plane channel, *Phys. Fluids* **5,** 545–549 (1962).
8. J. A. FAY, Plasma boundary layers, Massachusetts Institute of Technology Magnetohydrodynamics Laboratory, Report No. 61–8 (*AFOSR* 994) 1961.
9. D. MEKSYN, Magnetohydrodynamic flow past a semi-infinite plate, *J. Aerospace Sci.* **29,** 662–666 (1962).
10. I. TANI, Steady flow of conducting fluids in channels under transverse magnetic fields with consideration of Hall effect, *J. Aerospace Sci.* **29,** 297–305 (1962).
11. F. D. HAINS and Y. A. YOLER, Axi-symmetric magnetohydrodynamic channel flow, *J. Aerospace Sci.* **29,** 143–150 (1962).
12. W. C. MOFFATT, Boundary layer effects in magnetohydrodynamic flow, Mass. Inst. of Technology, MHD Laboratory Report No. 61–4, *AFOSR* 994 (1961).
13. G. L. CANN, Energy transfer processes in a partially ionized gas, California Institute of Technology, Pasadena, Calif., Memo No. 61, Army Ordnance Contracts No. DA-04-495-ORD-1960 and 3231 (1961).
14. M. D. NOVACK and T. R. BROGAN, Water-cooled insulating walls for MHD generators, *ASME* Paper 63-WA-348 (November 1963).
15. S. H. LAM, A general theory for the flow of weakly ionized gas, *AIAA J.* **2,** 256–262 (1964).
16. L. B. LOEB, *Basic Processes of Gaseous Electronics*, pp. 421, 478, 560. University of California Press, Berkeley, Calif. (1955).
17. H. SCHLICHTING, *Boundary Layer Theory*, Chapters 14, 15. McGraw-Hill, New York (1960).
18. H. N. OLSEN, Determination of properties of an optically thin argon plasma, in *Temperature—Its Measurement and Control in Science and Industry*, F. G. BRICKWEDDE, editor, Vol. 3, Part 1, pp. 593–606. Reinhold, New York (1962).
19. A. H. SHAPIRO, *Dynamics and Thermodynamics of Compressible Fluid Flows*, Vol. 2. Ronald Press, New York (1954).
20. J. O. HIRSCHFELDER, C. F. CURTIS and R. B. BIRD, *Molecular Theory of Gases and Liquids*. John Wiley, New York (1955).
21. S. C. LIN, E. L. RESLER, and A. KANTROWITZ, Electrical conductivity of highly ionized argon produced by shock waves, *J. Appl. Phys.* **26,** 95–109 (1955).
22. I. AMDUR and E. A. MASON, Properties of gases at very high temperatures, *Phys. Fluids* **1,** 370 (1958).
23. C. W. TAN, Thermodynamic and transport properties of non-equilibrium partially ionized monatomic gases, Ph.D. Thesis, University of Illinois (1963).
24. C. L. CHEN, C. C. LEIBY and L. GOLDSTEIN, Electron temperature dependence of the recombination coefficient in pure helium, *Phys. Rev.* **121,** 1391–1400 (1958).
25. J. M. BERGER, I. D. BERNSTEIN, E. A. FRIEMAN and R. M. KULSRUD, On the ionization and ohmic heating of a helium plasma, *Phys. Fluids* **1,** 297–300 (1958).
26. J. D. COBINE, *Gaseous Conductors*, p. 43. Dover Publications, New York (1958).
27. G. FRANCIS, *Ionization Phenomena in Gases*, pp. 54–56. Butterworth, Washington (1960).
28. D. R. BATES, *Atomic and Molecular Processes*, p. 267. Academic Press, New York (1962).
29. E. M. SPARROW, Analysis of laminar forced-convection heat transfer in entrance region of flat rectangular ducts, Nat. Advisory Comm. Aero. Tech. Note 3331 (January 1955).
30. K. STEPHAN, "Beitrag zur Berechnung des Wärmeüberganges and Druckabfalles laminarer Einlaufströmungen," *Ing. Arch.*, Vol. 29, p. 176–186 (1960).
31. W. M. ROHSENOW and H. T. CHOI, *Heat, Mass and Momentum Transfer*, p. 142. Prentice-Hall, Englewood Cliff, N.J. (1961).
32. W. J. PEARCE, Plasma jet temperature study, *TR*-59-346, Wright Air Development Center (1960).
33. R. G. NAGLER, Application of spectroscopic temperature measuring methods to definition of a plasma arc flame, Technical Report No. 32–66, Jet Propulsion Lab., California Inst. of Tech., Pasadena, California, (1961).
34. C. W. ALLEN, *Astrophysical Quantities*. Athlone Press, London (1955).
35. J. R. MCNALLY, JR., The direct-current experiment (DCX) and high temperature measurements in the carbon arc, in *Optical Spectrometric Measurements of High Temperatures*, P. J. DICKERMAN, editor, pp. 70–94. University of Chicago Press (1961).

APPENDIX A

Spectroscopic Measurements

The two-line method [32] was used in the determination of temperature and the method of electron continuum was used to calculate electron and ion densities [18, 33, 34].

The two-line method essentially makes use of the Saha intensity equation for two emission lines which are close together in wave length, but quite apart in energy levels. Comparison of the two emission intensities gives

$$T = \frac{(E_1 - E_2)/k}{\ln\left(\dfrac{A_1 g_1 \Lambda_2}{A_2 g_2 \Lambda_1}\right) - \ln\left(\dfrac{I_1}{I_2}\right)} \tag{A1}$$

where Λ_1, Λ_2 are two separate wavelengths close together; E_1, E_2 are particle energies; I_1, I_2 are line intensities; A_1, A_2 are transition probabilities; g_1, g_2 are statistical weights, all corresponding to Λ_1 and Λ_2 respectively, and k is the Boltzmann constant.

The electron number density may be obtained by a measure of the electronic continuum [34]. The relation, combined with Eggert–Saha equation gives

$$n_e = \frac{Z_i\ I_a\ A_i\ g_i\ \Lambda_i}{Z_a\ I_i\ A_a\ g_a\ \Lambda_a}\ \frac{(2\pi m_e kT)^{3/2}}{h^3} \exp\left[-(E_I + E_i - E_a)/kT\right] \qquad \text{(A2)}$$

where I_a/I_i is the ratio of emission intensities; A_a/A_i is the ratio of transition probabilities; g_a/g_i is the ratio of statistical weights, all of an atomic and ionic line of the same element; Z_i/Z_a is the ratio of their partition functions; E_I is the ionization energy of first degree; E_a is the atom particle energy; and E_i is the ion particle energy. Also, from the Saha equation, the ion number density can be calculated according to [35]:

$$n_i = \frac{2(2\pi m_e kT)^{3/2}}{h^3}\ \frac{n_a}{n_e}\ \frac{g_i}{g_a} \exp\left[-E_I/kT\right]$$

$$= 2\frac{Z_a}{Z_i} n_a \frac{I_i}{I_a}\ \frac{A_a}{A_i}\ \frac{\Lambda_i}{\Lambda_a} \exp\left[-(E_a - E_i)/kT\right] \qquad \text{(A3)}$$

where the notations are similar to those of equation (A2).

APPENDIX B

Iterative Solution

By taking $j = 0, 1$ in equations (19) and (20), determining the coefficients from the boundary conditions for velocity and temperature, one finds

$$\frac{u}{u_1} = f(\eta^*) = \eta^* \qquad \text{(B1)}$$

$$\frac{T}{T_1} = g(\eta) = b_0 + b_1\eta \qquad \text{(B2)}$$

where $b_0 = T_w/T_1$.

Utilizing equations (B1) and (B2), δ^*, θ, θ_H, $(\partial u/\partial y)_w$ and $(\partial T/\partial y)_w$ can be evaluated and substituted in equations (1) and (2), which become, respectively,

$$\frac{d\delta_1}{dx} = -\frac{1}{u_1}\frac{du_1}{dx}\left[4\delta_1 - 3(1 - b_0)\Delta_1\right] + \frac{6\mu_w}{\rho_1 u_1}\ \frac{1}{b_0\delta_1} \qquad \text{(B3)}$$

$$\left.\begin{aligned} \frac{dw_1}{dx} = \frac{3}{2}\Bigg[&\frac{1}{\delta_1}\frac{d\delta_1}{dx} - \frac{b_0}{1-b_0}\ \frac{1}{\rho_1 u_1 h_1}\ \frac{d}{dx} (\rho_1 u_1 h_1)\Bigg] w_1 + \frac{9\mu_w}{Pr_w}\ \frac{\delta_1}{\rho_1 u_1 b_0} \\ &- \frac{9\delta_1\Delta_1^2}{\rho_1 u_1 h_1(1-b_0)}\left[\frac{1}{2} - \frac{1}{\gamma_1} + \frac{1-b_0}{6\gamma_1^2} + \frac{1}{\gamma_1(1-b_0)}\int_{b_0}^{1} g\frac{\sigma}{\sigma_1}dg\right] E^2\sigma_1 \end{aligned}\right\} \text{(B4)}$$

if $\delta_1 > \Delta_1$, or

$$\left(\frac{\gamma_1^2}{6} - \frac{1}{2}\right)\frac{d\Delta_1}{dx} = -\left(\frac{1}{2} - \frac{\gamma_1}{3}\right)\frac{d\delta_1}{dx} - \frac{\mu_w}{Pr_w}\ \frac{1}{\rho_1 u_1 b_0}\ \frac{1}{\Delta_1} - \left[\frac{b_0}{(1-b_0)}\ \frac{1}{\rho_1 u_1 h_1}\ \frac{d}{dx}(\rho_1 u_1 h_1)\right]\left(-\frac{1}{2} + \frac{\gamma_1}{2} - \frac{\gamma_1^2}{6}\right)\Delta_1$$
$$+ \frac{\Delta_1}{\rho_1 u_1 h_1(1-b_0)}\left[\frac{b_0}{2}\gamma_1 - \frac{1+b_0}{2} + \frac{1-b_0}{2}\gamma_1^2 + \frac{1}{1-b_0}\int_{b_0}^{1} g\frac{\sigma}{\sigma_1}dg\right] E^2\sigma_1 \qquad \text{(B5)}$$

if $\Delta_1 > \delta_1$, where $w_1 = \Delta_1^3$.

Along with these equations are to be included equations (10), (23), and (25) which, by considering the velocity and the temperature profiles of equations (B1) and (B2), are, respectively:

$$\frac{1}{T_1}\ \frac{dT_1}{dx} = \frac{E^2\sigma_1}{\rho_1 u_1 h_1} \qquad \text{(B6)}$$

$$\dot{m} = 2a\ \rho_1 u_1\left[b - \frac{1}{2}\delta_1 + \frac{1-b_0}{2}\Delta_1\right] \qquad \text{(B7)}$$

$$I = 2a\,E\,\sigma_1 \left[b - \Delta_1 \left(\frac{1+b_0}{2} - \frac{1}{1-b_0} \right) \int_{b_0}^{1} g \frac{\sigma}{\sigma_1}\, dg \right] \quad \text{(B8)}$$

Solution of the momentum and integral equations

To obtain $\delta_1(x)$, $\Delta_1(x)$, $u_1(x)$, $T_1(x)$ and $\sigma(T)$ from the five equations of (B3), (B4) (or (B5) if $\Delta_1 > \delta_1$), (B6), (B7), and (B8), select the first two terms of a Taylor series expansion of δ_1, Δ_1, u_1, and T_1, such as

$$\delta_{1u} = \delta_{1m} + \left(\frac{d\delta_1}{dx}\right)_m \Delta x, \quad \text{etc.} \quad \text{(B9)}$$

where $n = m + 1$ and Δx is a small interval. The five equations noted are solved simultaneously by the iteration method explained below:

1. Assume a relation for $\sigma(T)$. As a logical choice, select $\sigma(T)$ given for thermally ionized argon gas by [21]

$$\sigma = 7{\cdot}65 \times 10^{-5}\, T^{3/4} \frac{1}{Q} \exp[-91000/T] \quad \text{(B10)}$$

where Q is the collision cross-section. Taking Q to be independent of T, then

$$\frac{\sigma}{\sigma_1} = \left(\frac{T}{T_1}\right)^{3/4} \exp\{(-91000/T_1)\,[(T_1/T) - 1]\} \quad \text{(B11)}$$

2. Evaluate

$$\int_{b_0}^{1} g \frac{\sigma}{\sigma_1}\, dg = \int_{b_0}^{1} g^{7/4} \exp\{(-91000/T_1)\,[(1/g) - 1]\}\, dg \quad \text{(B12)}$$

graphically for various values of T_1.

3. Take in each small interval of Δx, $\rho_1 u_1$ to be constant, thus,

$$\frac{1}{\rho_1 u_1 h_1} \frac{d}{dx}(\rho_1 u_1 h_1) \approx \frac{1}{T_1}\frac{dT_1}{dx} \quad \text{(B13)}$$

and, by neglecting dp/dx,

$$\frac{1}{u_1}\frac{du_1}{dx} \approx \frac{1}{T_1}\frac{dT_1}{dx} \approx \frac{E^2 \sigma_1}{\rho_1 u_1 h_1} \quad \text{(B14)}$$

4. Solve equations (B3) and (B4) if $\delta_1 > \Delta_1$ and equations (B3) and (B5) if $\Delta_1 > \delta_1$ along with equations (6B), (B7) and (B8), using equation (B12). The solutions will give δ_1, Δ_1, T_1, u_1 as functions of x and σ_1 as a function of T_1, or σ as a function of T.

5. With the values of σ thus obtained evaluate

$$\int_{b_0}^{1} g \frac{\sigma}{\sigma_1}\, dg$$

graphically as before and repeat steps 1 to 4 to obtain new values of δ_1, Δ_1, u_1, T_1 and σ_1.

Repeat step 5 until the difference in values of σ_1 between the two iterations is very small (σ_1 converged).

The number of iterations

Since the values of σ originally assumed are changed to the next step of the iteration it is clear that the accuracy of σ originally used reduces the number of iterations.

It is found that $\sigma(T)$ converges rather rapidly and not more than three iterations are needed (Fig. 24).

The final values of $\sigma(T)$ obtained by using the test section at atmospheric pressure are used as

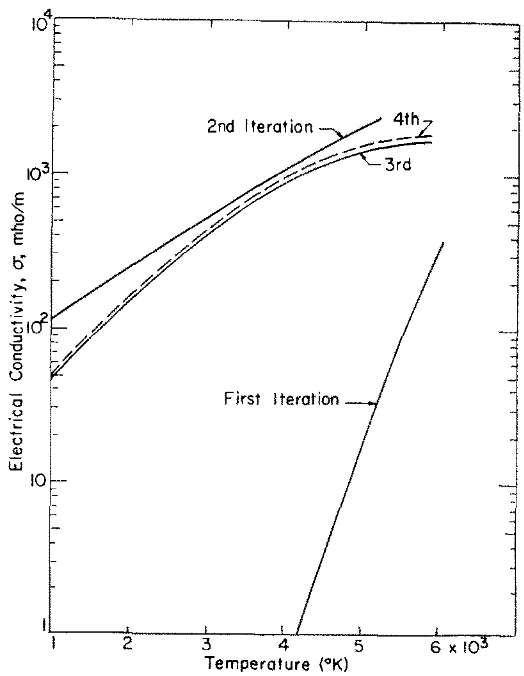

FIG. 24. Iterated electrical conductivity.

the first iteration for the test section at lower pressures.

For each interval $\Delta x = 10^{-3}$ m taken for the numerical integration the following energy balances are checked:

Energy crossing section n:

$$Q_n = 2a\left\{\rho_1 u_1 h_1 \left[b - \left(\frac{b_0}{2} + \frac{1-b_0}{2}\gamma_1\right)\delta_1\right]\right\} \tag{B15}$$

Heat loss between sections m and n

$$Q_{mn} = a\frac{\mu_w}{Pr_w}\left[\left(\frac{h_1}{\Delta_1}\frac{1-b_0}{b_0}\right)_m + \left(\frac{h_1}{\Delta_1}\frac{1-b_0}{b_0}\right)_n\right]\Delta x \tag{B16}$$

With the energy balance of

$$(V_n - V_m)I = Q_n - Q_m + Q_{mn} \tag{B17}$$

the thermal conductivity $\lambda_w = (\mu_w/Pr_w)c_p$ in equation (B16) is taken (after several additional iterations) such that

$$\int_0^1 Q_n\,dx \tag{B18}$$

gives the total heat losses to the walls, determined by measuring the cooling water flow rate and its temperature rise.

Once the above iteration procedure is completed and λ_w is determined, the thermal conductivity is given by:

$$\lambda = \lambda_w\frac{T}{T_w} + E^2\sigma_1\left[\frac{\Delta_1}{(1-b_0)T_1}\right]^2 T\int_{b_0}^{g} g\frac{\sigma}{\sigma_1}\,dg \tag{B19}$$

The viscosity is determined in a similar manner via:

$$\mu\frac{\partial u}{\partial y} = \mu_w\left(\frac{\partial u}{\partial y}\right)_w - \rho_1 u_1 u_1' y - u\int_0^y \frac{\partial}{\partial x}(\rho u)\,dy + \int_0^y\left[\rho u\frac{\partial u}{\partial x} + u\frac{\partial}{\partial x}(\rho u)\right]dy \tag{B20}$$

Résumé—Les propriétés de transport en non-équilibre de l'argon partiellement ionisé et la nature de la relaxation des électrons sur une surface refroidie ont été étudiés à l'aide de mesures effectuées dans un écoulement permanent chauffé par un arc dans une conduite bidimensionnelle. L'étude consiste en une extension de la théorie de la couche limite au cas de l'écoulement d'un gaz ionisé sur une paroi refroidie, et en l'évaluation des propriétés de transport à l'aide d'une solution par itération des équations globales de la quantité de mouvement. Les résultats montrent que, bien que les températures atomique et ionique diminuent sensiblement vers la paroi refroidie, la température et la concentration électroniques ainsi que les conductivités thermique et électrique demeurent à des valeurs beaucoup plus élevées que celles basées sur la concentration électronique à l'équilibre.

Zusammenfassung—Transporteigenschaften im Nichtgleichgewicht für teilweise ionisiertes Argon und die Natur der Elektronenrelaxation an einer kalten Oberfläche wurden mit Hilfe von Messungen an einem stationären Strom in einem zweidimensionalen bogenbeheizten Kanal untersucht. Die Untersuchung besteht aus der Erweiterung der Grenzschichttheorie auf die Strömung eines ionisierten Gases über eine gekühlte Wand und der Abschätzung der Transporteigenschaften nach einer iterativen Lösungsmethode der Impuls-Integralgleichungen. Die Ergebnisse zeigen, dass trotz der deutlichen Abnahme der Atom- und Ionentemperatur in Richtung der gekühlten Wand, die Elektronentemperatur, die Konzentration und die thermische und elektrische Leitfähigkeit viel höhere Werte beibehalten als auf Grund der Gleichgewichtselektronenkonzentration ermittelt werden.

Аннотация—Изучались характеристики неравновесного переноса частично ионизированного аргона и природа релаксации электронов на охлажденной поверхности, причем измерения проводились при стационарном течении в двумерном канале, нагреваемом дугой. Теория пограничного слоя развивалась на случай течения ионизированного газа на охлажденной стенке. Характеристики переноса вычислялись с помощью численного метода итерации на основе интегрального уравнения нереноса импульса. Результаты показывают, что температура атома и иона значительно понижается при приближении к охлаждаемой стенке, температура электрона, концентрация, тепло-и электропроводность остаются намного выше значений, полученных в том случае, когда за основу бралась равновесная концентрация электронов.